

Supporting Information

Polyethylenimine Assisted Non-Monotonic Jamming of silica Colloids during Evaporation Induced Assembly and its Implication on CO₂ Sorption Characteristics

Swati Mehta^{1,2}, Jitendra Bahadur^{1,2*}, Debasis Sen^{1,2}, Saideep Singh³, Vivek Polshettiwar³

¹Solid State Physics Division, Bhabha Atomic Research Centre, Mumbai, 400085, India

²Homi Bhabha National Institute, Anushaktinagar, Mumbai, 400094, India

³Department of Chemical Science, Tata Institute of Fundamental Research, Mumbai, 400001, India

Chemical Details of Polyethylenimine:

Polyethylenimine is a low to high molecular weight polymer with a monomer unit of $-\text{[CH}_2\text{-CH}_2\text{-NH}_2\text{]}-$. PEI is available as linear, branched as well as in dendrimer structures. Linear PEI is obtained via ring-opening polymerization of 2-ethyl 2-oxazoline followed by hydrolysis whereas, branched PEI is synthesized via acid-catalyzed polymerization of aziridine. Linear PEI contains only primary amines, however, branched PEI consists of primary, secondary as well as tertiary amines in the ratio of 1:2:1. PEI is a cationic polyelectrolyte with a charge depending on the pH of the dispersion. The Schematic of PEI is shown in Fig. S1.

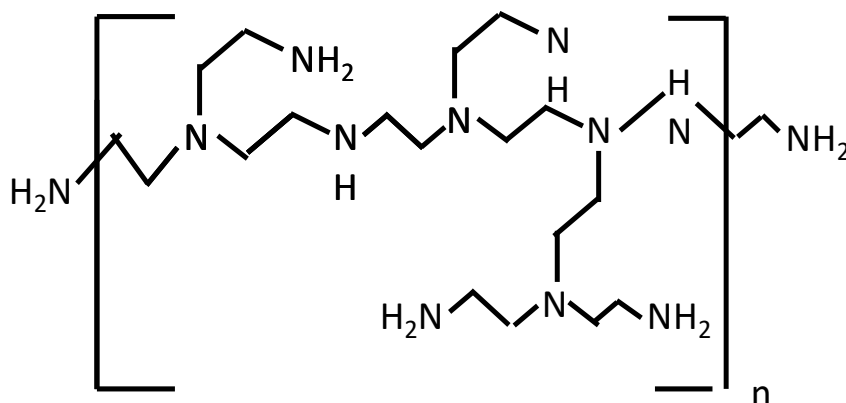


Figure S1: Schematic of the branched structure of polyethylenimine.

In the present case, branched PEI of molecular weight 0.8kg/mol, having a zeta potential of +3.8 mV at pH of 10.5, was used for the preparation of samples.

Fourier transform of High-Resolution FESEM images

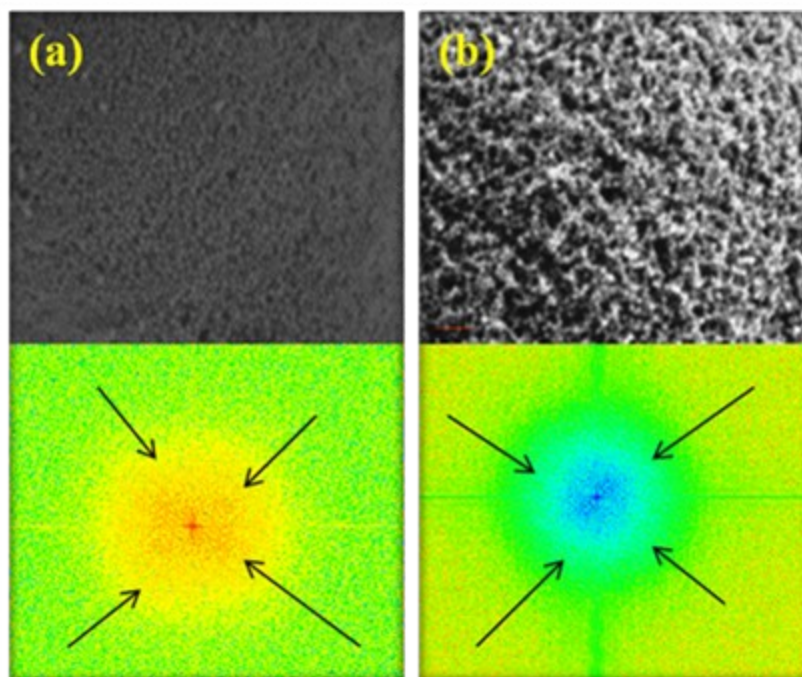


Figure S2: Fast Fourier Transform (FFT) of FESEM images for silica and silica-PEI microspheres. (a) HS40 (b) HS40-PEI (5). Arrows are for the sake of clarity to indicate the low Q region (blue). High intensity in b) refers to the formation of clusters whereas low intensity in a) depicts the uniform jamming in silica-PEI microspheres.

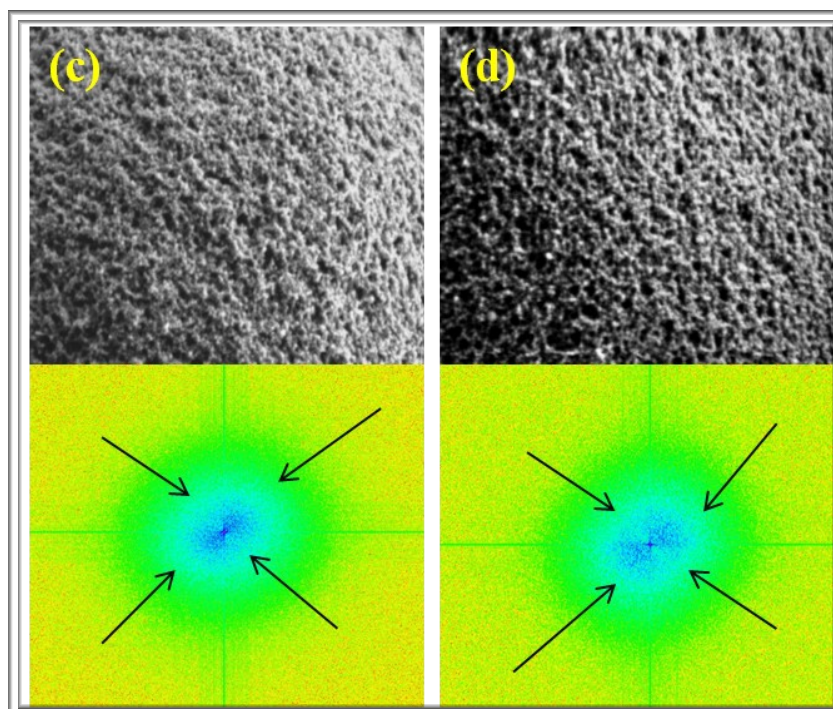


Figure S3: Fast Fourier Transform (FFT) of FESEM images for silica-PEI microspheres. (a) HS40-PEI (20) (b) HS40-PEI (33). Arrows are for the sake of clarity to indicate a low Q region (blue). The presence of the high-intensity region indicates the presence of nanoparticle clusters.

Line Plot Analysis of High-Resolution FESEM images

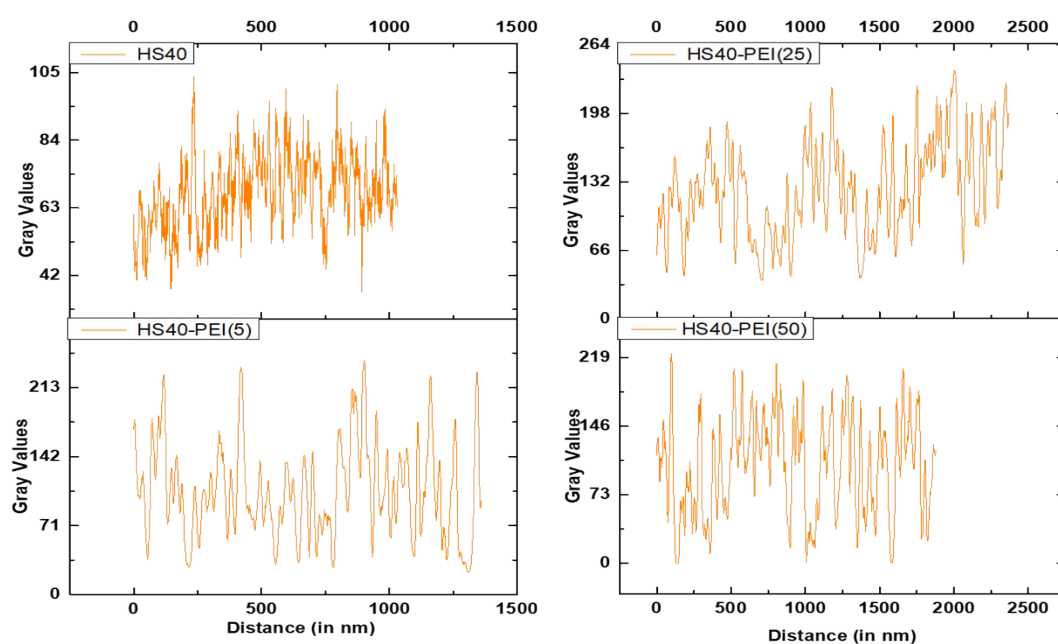


Figure S4: Profile plot of the electron microscopy high-resolution images of silica and PEI incorporated silica shown in Figures S1 and S2.

SAXS data for HS40-PEI(50) microspheres from Lab-based X-ray Source

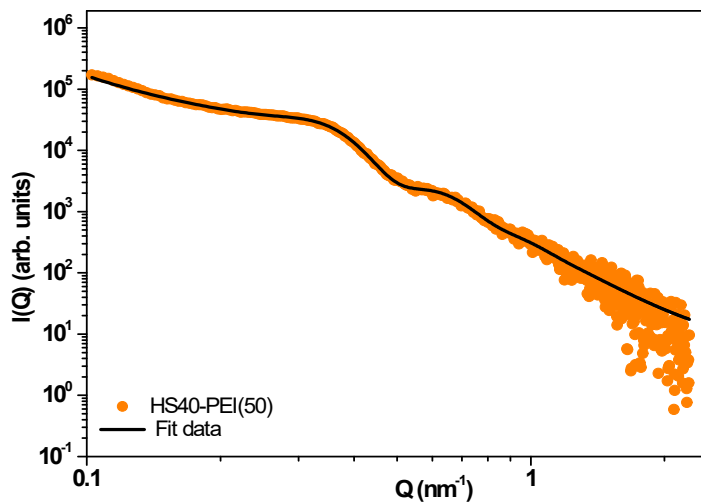


Figure S5: SAXS Profiles of HS40-PEI(50) microspheres. A solid line shows the model fit to the data.

Size distribution of HS40 microspheres obtained from fitting of SAXS data

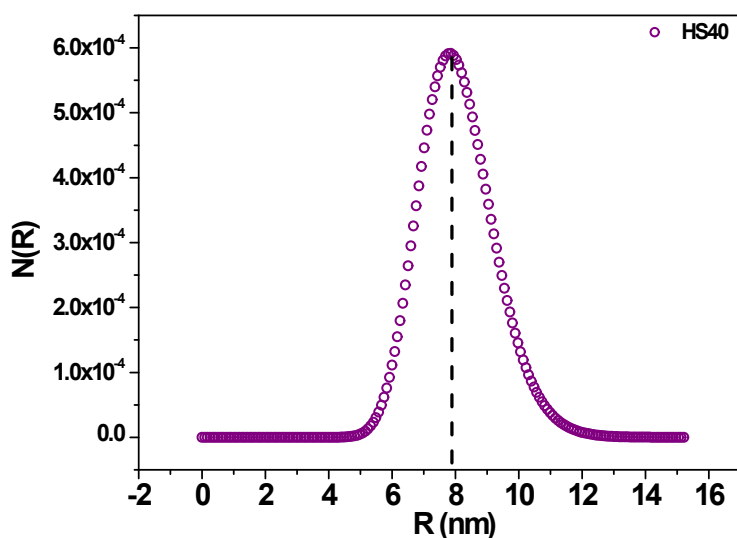


Figure S6: Particle Size distribution of virgin silica colloids obtained using the model fit of SAXS profiles. Maxima in particle size distribution represents the average radius of silica nanoparticles.

Estimation of Specific Interface area between jammed silica nanoparticles: Calculation of the composite density

Let's take m mass of silica microspheres then $PEI(x) \times m$ is the mass of the PEI, where x is the polymer concentration.

Let V_s and V_p be the volume of the silica nanoparticles and PEI respectively, which is given as

$$V_s = \frac{m}{d_s \times \phi_s} \quad \text{and} \quad V_p = \frac{PEI(x) \times m}{d_p}$$

(a)

d_s and d_p are the densities of the silica nanoparticles and PEI, respectively.

$$\phi_s = \frac{\frac{m}{d_s \times \phi_s}}{\frac{m}{d_s \times \phi_s} + \frac{PEI(x)m}{d_p}} \phi_p = \frac{\frac{PEI(x) \times m}{d_p}}{\frac{m}{d_s \times \phi_s} + \frac{PEI(x) \times m}{d_p}}$$

Therefore,

(b)

ϕ_s and ϕ_p are the volume fractions of the silica microspheres and PEI. ϕ_s is the volume fraction of the silica obtained through the model fitting of SAXS profiles.

$$\text{Hence, Composite density, } d_c = d_s \times \phi_s \times \phi + d_p \times \phi_p \quad \text{(c)}$$

The interfacial area between the jammed nanoparticles in the solid nano-adsorbent from the fitting parameters of SAXS profiles can be calculated using the equations below:

$$\frac{\Sigma}{d_c} = \frac{\left[\lim_{q \rightarrow \infty} I(Q)Q^4 \right]}{2\pi d_c (\Delta\rho)^2} \quad (d)$$

$$Q_{inv} = \int_0^{\infty} I(Q)Q^2 dQ = 2\pi^2 \phi_s (1 - \phi_s) \Delta\rho^2 \quad (e)$$

$$\frac{\Sigma}{d_c} = \frac{\left[\pi \phi_s (1 - \phi_s) \left[\lim_{q \rightarrow \infty} I(Q)Q^4 \right] \right]}{Q_{inv} d_c}$$

(f) Where, Σ/d_c is specific surface area (m^2/g), ϕ_s is the volume fraction of silica nanoparticles and d_c (g/cm^3) (eq. (c)) is the density of PEI-silica microspheres. $\lim_{q \rightarrow \infty} I(Q)Q^4$ is the Porod constant obtained from the Porod plot ($I(Q)Q^4$ vs. Q) of the SAXS data of HS40-PEI microspheres at different loading of PEI, Fig. S7a. The high- Q region in the Porod plot tends to horizontal asymptote indicating sharp interfaces whereas the bell shape of the Kratky plot ($I(Q)Q^2$ vs. Q), Fig. S8 suggests that the Q_{inv} integral is converging.

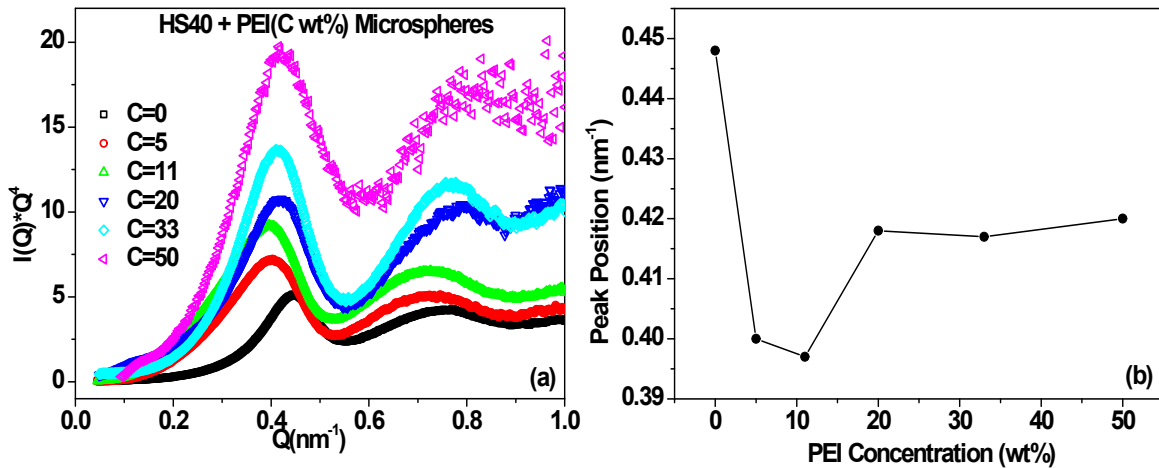


Figure S7: (a) Porod plot for the pure silica and PEI- functionalized silica. Data is shifted vertically for the clarity purpose. (b) Non-monotonic behaviour of the peak position with variation in the concentration of PEI.

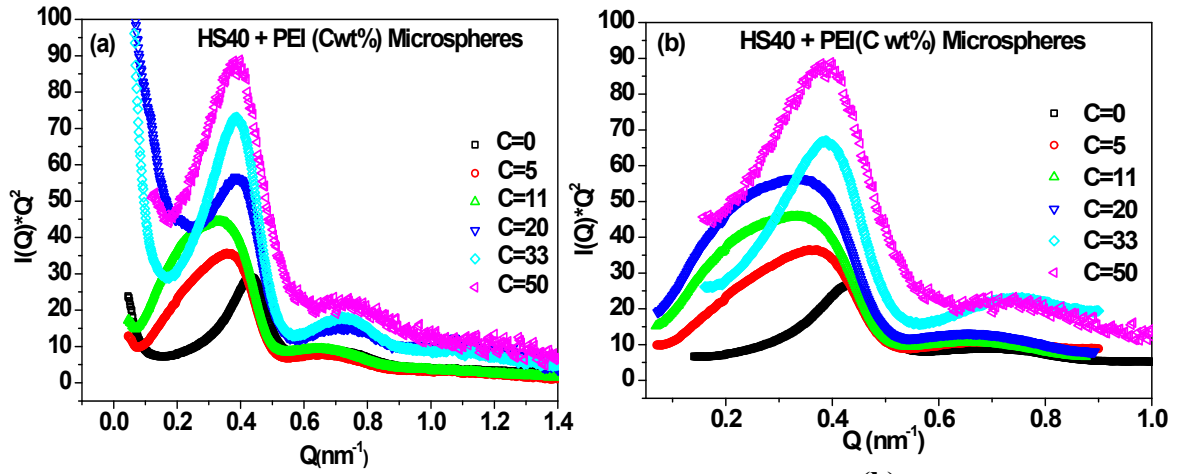


Figure S8: Kratky plot for pure silica and PEI-functionalized silica. Data is shifted vertically for a clear presentation. (b) The Low Q region is subtracted.

BET (Brunauer-Emmett-Teller) and BJH (Barrett, Joyner, and Halenda) analysis of N_2 adsorption isotherms:

BET (Brunauer-Emmett-Teller) theory is applied to calculate specific surface area using N_2 gas adsorption. BET equation is given as¹,

$$\frac{1}{v \left(\frac{p_0}{p} - 1 \right)} = \frac{1}{v_m c} + \frac{c-1}{v_m c} \left(\frac{p}{p_0} \right)$$

(g)

Here, v is the number of molecules adsorbed at a given temperature. v_m is the number of gas molecules/atoms required to form a monolayer on a solid surface. p_0 is the saturation pressure and p is the equilibrium pressure of the nitrogen gas at 77K.

$$\frac{1}{v \left(\frac{p_0}{p} - 1 \right)} \text{ Vs. of } \frac{p}{p_0} \text{ gives a straight line with}$$

$$v_m = \frac{1}{\text{slope} + \text{intercept}} \quad c = 1 + \frac{\text{slope}}{\text{Intercept}}$$

(h)

Therefore, the total surface area and specific surface area is given by

$$S_{Total} = \frac{sN_A v_m}{V} \quad S_{BET} = \frac{S_{Total}}{a} \quad (i)$$

Where, s is the adsorbing cross-section of silica microspheres, N_A Avogadro's number and a is the mass of the silica nanoparticles.

BJH (Barrett, Joyner, and Halenda) method² is employed to calculate pore size distribution using adsorption-desorption isotherm by utilizing the Kelvin equation, given as

$$r_K = \frac{-2\sigma v_1}{RT \ln\left(\frac{p}{p_0}\right)}$$

(j)

Here, r_K is the Kelvin radius. σ and v_1 are the surface tension and molar volume of the liquid condensate, respectively. R is the gas constant and T is the temperature.

The Kelvin radius obtained from eq. (j) determines the pore radius and the film thickness of the adsorbed multilayer obtained using standard isotherms as:

$$r = r_K + t \quad (k)$$

Multimodal Peak Analysis of Pore volume distribution:

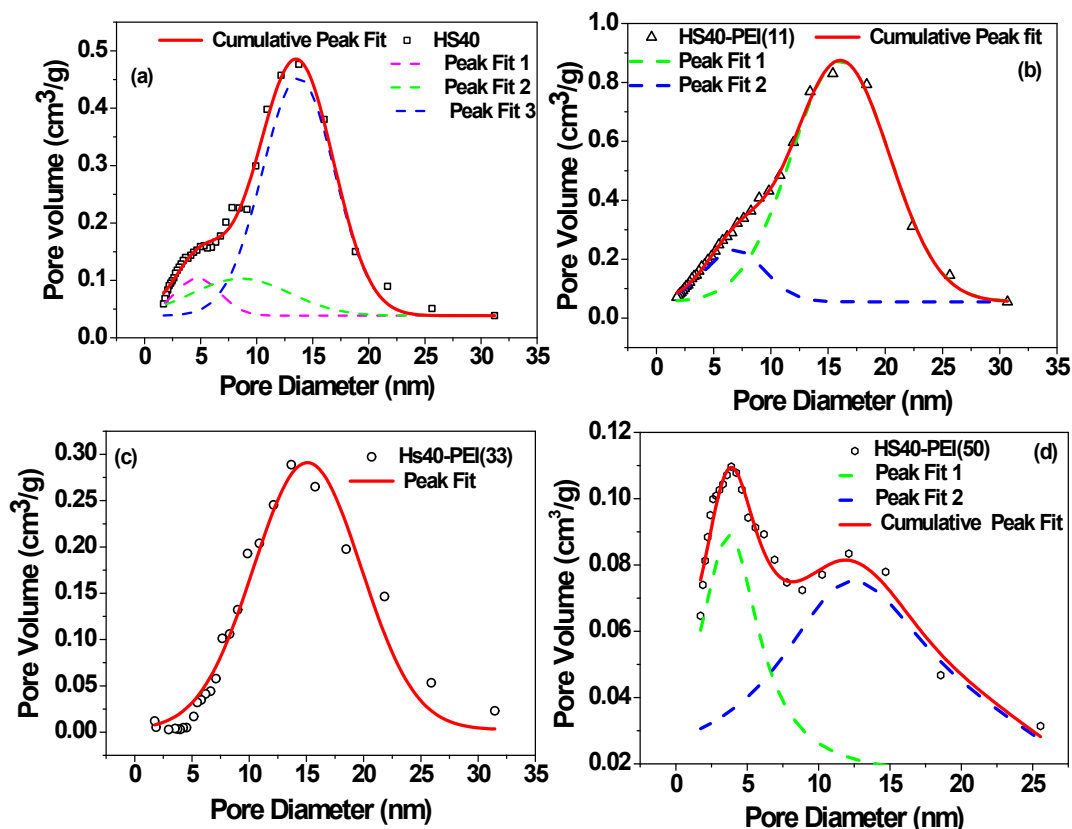


Figure S9: Multimodal to monomodal peak analysis of (a) HS40 (b) HS40-PEI(11) (c) HS40-PEI(33) (d) HS40-PEI(50) microspheres.

Zeta potential measurements:

The pH of the dispersions for all loading of PEI was measured at ~ 10 . The zeta potential measured for bare silica colloids is estimated to be ~ -45 mV whereas the PEI dispersion shows positive zeta potential (~ 3.8 mV) at pH ~ 10.5 . Due to the presence of a large number of amine groups, the surface charge of PEI is positive. The zeta potential of silica colloids is negative with the magnitude of negative charge decreasing as the concentration of PEI is increased.

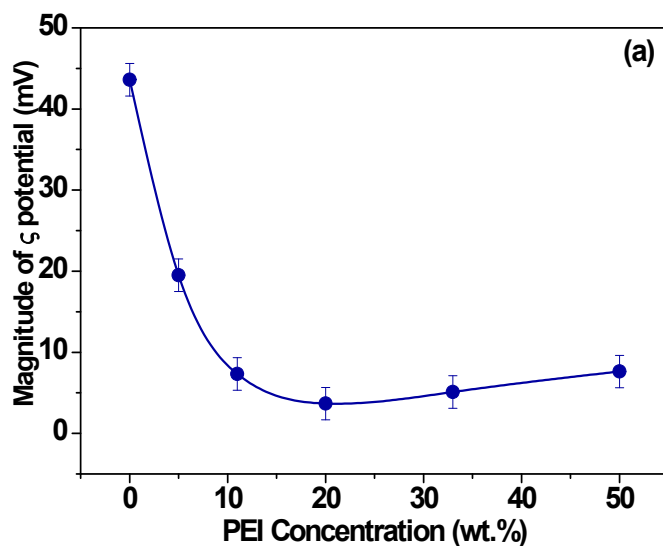


Figure S10: (a) Zeta potential for 2wt% HS40-PEI dispersion with the variation in the concentration of PEI. (b) SANS data for 1 wt% HS40 for different concentrations of PEI.

Thermo-gravimetric Stability Analysis

Table S1: The variation in the bound water wt% for different PEI loadings using thermo-gravimetric analysis.

Sample	HS40	HS40- PEI(5)	HS40- PEI(11)	HS40- PEI(20)	HS40- PEI(33)	HS40- PEI(50)
Total weight loss (wt%)	5	14	17	25	36	44
Weight loss due to bound water and silanol groups (wt%)	5	9	6	5	3	-

Calculation of potential amine sites:

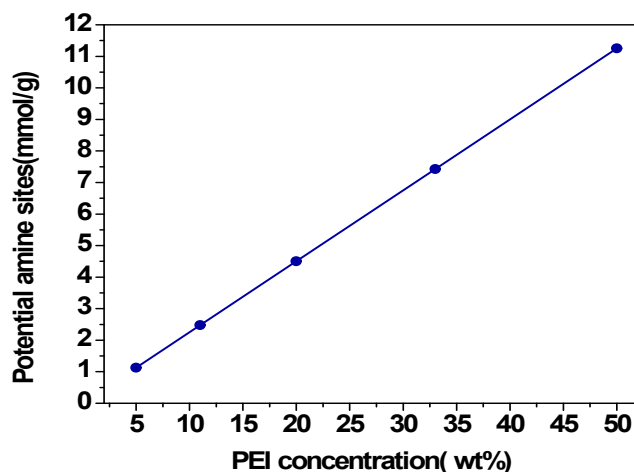


Figure S11 : Potential amine sites over silica-PEI microspheres as a function of PEI loading.

Wang et. al.³ calculated the potential amine sites for the PEI loaded in the sorbent removing the contribution from the surface silanol groups consuming the part of the loaded PEI. However, in the present case, PEI is adsorbing on the silica nanoparticles via electrostatic attraction therefore, the modified formula to calculate amine sites in a sorbent is given as:

$$\text{Potential amine sites} \left(\frac{\text{mol}}{\text{g}} \right) = \text{Wt\% of the PEI in the sorbent} \times \frac{n}{M_{W_{PEI}}} \quad (1)$$

Here, $M_{W_{PEI}}$ is the molecular weight of PEI, 0.8kg/mol and n is 18, the number of amine groups in each PEI chain.

CO₂ capture capacity with the variation in temperature

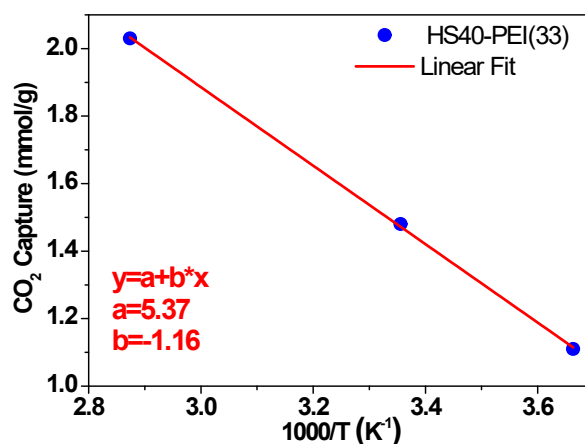


Figure S12: CO₂ capture for HS40 microspheres at different temperature using volumetric adsorption

CO₂ Capture Capacity with the Variation in the PEI loading

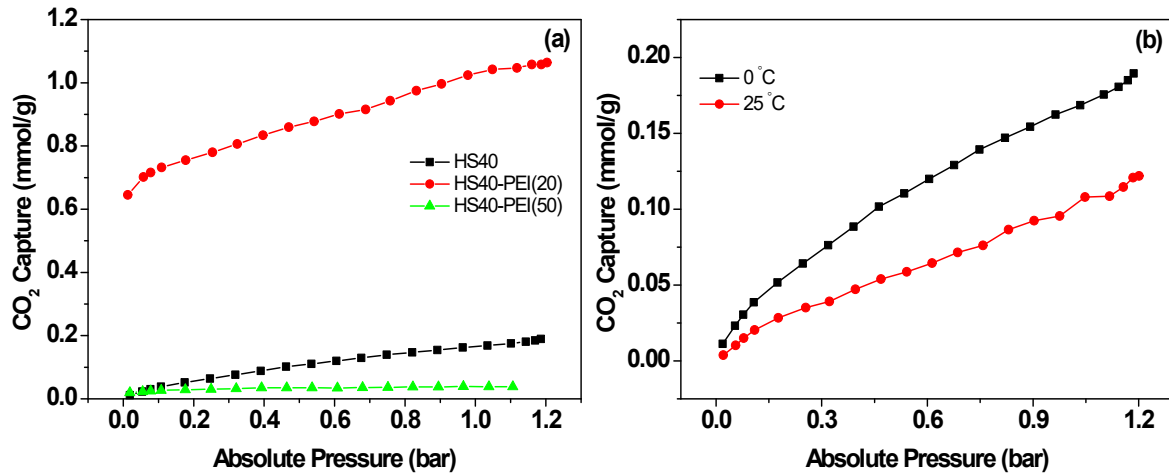


Fig. S13 CO₂ capture for (a) different loadings of PEI at 0 °C (b) HS40 microspheres at 0 °C and 25 °C using volumetric adsorption.

Modelling of CO₂ adsorption isotherms

Langmuir Model:

The Langmuir model describes the adsorption on a homogeneous surface by monolayer formation⁴. The assumptions considered by the Langmuir model: 1) adsorbate should be energetically homogeneous, 2) one site occupies one adsorbed molecule, and 3) adsorbed molecules should not have lateral interaction. Therefore, the Langmuir model of adsorption isotherm is described as⁵:

$$q_e = \frac{q_L k_L p}{1 + k_L p} \quad (m)$$

Here, q_L (mmol/g) is the adsorption capacity of the monolayer, p (bar) is the pressure and k_L (bar^{-1}) represents the affinity constant related to the energy of the adsorption. Furthermore, a dimensionless parameter (R_L), known as the separation factor, defined by Weber and Chakarvorti⁶, is represented as:

$$R_L = \frac{1}{1 + K_L p} \quad (\text{n})$$

Separation factors indicate the adsorption nature to be linear ($R_L=1$), irreversible ($R_L=0$), unfavourable ($R_L>1$), or favourable ($0<R_L<1$).

Sips Model:

The Sips model has three parameters, which is a combination of both the Freundlich and Langmuir models. Sips model is suitable for envisaging adsorption on the heterogeneous surfaces following the homotattic patch approximation (HPA), described as⁵:

$$q_e = \frac{q_S (k_s p)^{\frac{1}{m_s}}}{1 + (k_s p)^{\frac{1}{m_s}}} \quad (\text{o})$$

Here, k_S (bar^{-1}) is the affinity, m_S is the heterogeneity factor. A value of m_S near to 1 represents the homogenous adsorption sites where $m_S < 1$ represents the possession of heterogeneous adsorption sites by the adsorbent⁵. When m_S equals to 1, the Sips model is reduced to the Langmuir model.

Freundlich Model:

Freundlich model follows homotattic patch approximation (HPA), proposed by Ross and Olivier⁷, where the adsorbent's heterogeneous surface is sub-divided into finite homogeneous

patches, each having different site energy forming the energy distribution function over the surfaces. Therefore, an empirical equation is used to describe the Freundlich model, which is reported as⁵:

$$q_e = k_f p^{\frac{1}{n}} \quad n = \frac{-\Delta H_{ad}}{RT} \quad (p)$$

Here, q_e is the CO₂ capture capacity (mmol/g), k_f (mmol g⁻¹ bar^{-1/n}) is the constant of the Freundlich isotherm, p is the pressure (bar) and n represents the deviation from the linearity of the adsorption. n indicates the relative distribution of the energy and heterogeneity of the adsorption sites and predicts the favourability of the adsorption. ΔH_{ad} (kJ/mol) is the heat of adsorption, R (8.314 J mol⁻¹ K⁻¹) is the universal gas constant; T (K) is the temperature.

Table S2: Parameters of the Freundlich, Langmuir and Sips isotherms for CO₂ adsorption of silica-PEI microspheres at different loading of PEI and at different temperatures.

Models	Parameters	Samples			
		HS40- PEI(11)	HS40- PEI(11)	HS40- PEI(33)	HS40- PEI(33)

		At 0°C	At 75°C	At 0°C	At 75°C
Freundlich	k_f	0.31	0.38	0.38	0.47
	n	1.41	1.47	1.38	1.53
	-ΔH_{ad}(kJ/mol)	3.0	4.25	3.13	4.57
	R²	0.996	0.996	0.996	0.989
Langmuir	q_L	1.09	1.91	0.98	1.93
	k_L	0.36	0.21	0.64	0.28
	R²	0.992	0.990	0.991	0.979
Sips	q_s	1.86	1.55	2.13	1.45
	k_s	0.2	0.35	0.35	0.35
	m_s	1.25	1.34	1.55	0.79
	R²	0.991	0.988	0.987	0.973

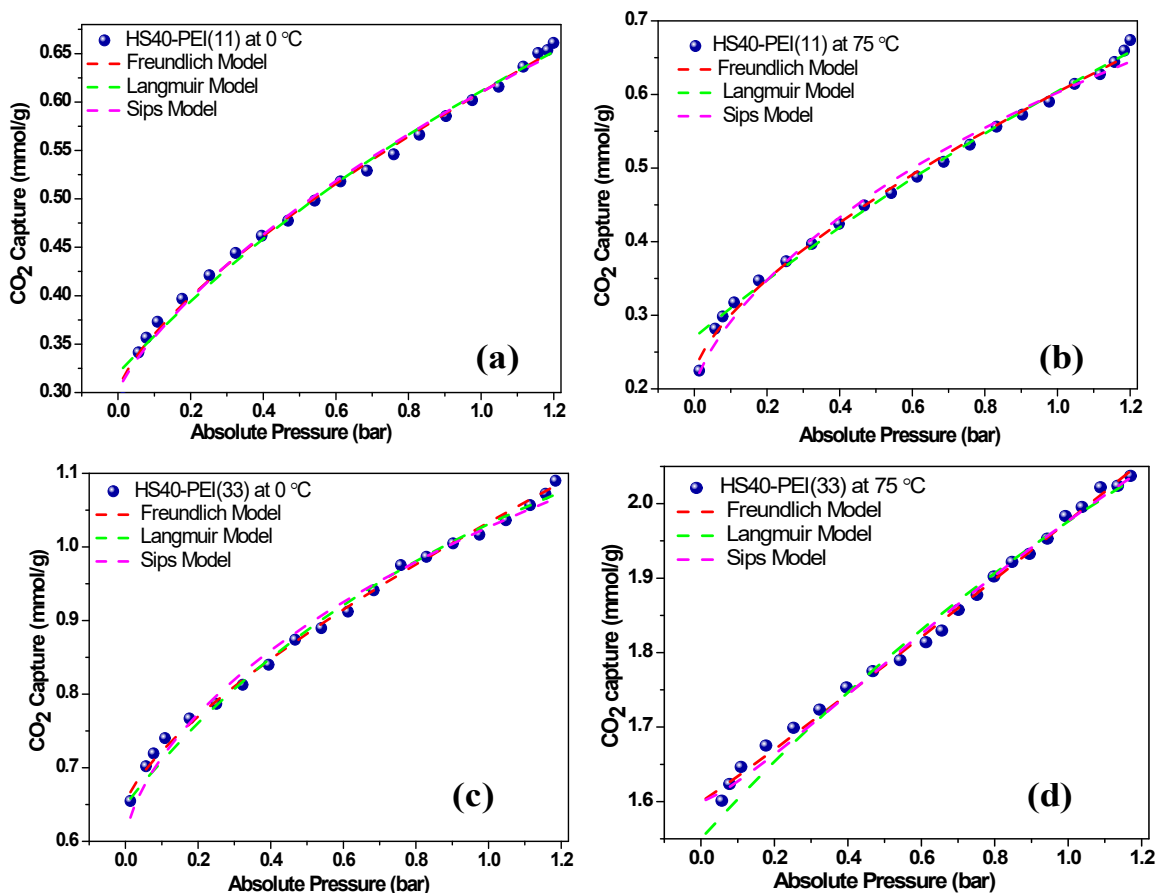


Figure S14: Fitting of the experimental data of the CO₂ adsorption isotherm to the various theoretical models for (a-b) HS40-PEI(11) and (c-d) HS40-PEI(33) at different temperatures.

Table S3: Comparison of the various sorbents PEI-silica composites.

Sorbent	Temperature (°C)	CO ₂ Pressure	Sorption capacity (mg/g)	Ref.
HS40-PEI(50)	75	1	89.8	This study
Silica gel-PEI(50)	75	1	78	8
SBA15-PEI(50)	75	1	89.8	9
SBA15-PEI(50)	75	5.5	95.4	9
I-SBA-15-PEI(50)	75	1	74.6	10
MCM41-PEI(30)	75	-	68.7	11
MCM41-PEI(50)	75	-	112	11
KCC1-PEI(LMW)(33wt%)	50	-	79.6	12
Fumed silica-PEI(50)	85	1	156	13

References:

1. D. Dollimore, P. Spooner and A. Turner, *Surface Technology*, 1976, **4**, 121-160.
2. E. P. Barrett, L. G. Joyner and P. P. Halenda, *Journal of the American Chemical society*, 1951, **73**, 373-380.
3. X. Wang, X. Ma, C. Song, D. R. Locke, S. Siefert, R. E. Winans, J. Mollmer, M. Lange, A. Moller and R. Glaser, *Microporous and Mesoporous Materials*, 2013, **169**, 103-111.
4. G. McKay, A. Mesdaghinia, S. Nasser, M. Hadi and M. S. Aminabad, *Chemical Engineering Journal*, **251**, 236-247.
5. J. R. Guarin Romero, J. C. Moreno-Pirajan and L. Giraldo Gutierrez, *C*, 2018, **4**, 52.
6. T. W. Weber and R. K. Chakravorti, *AIChE Journal*, 1974, **20**, 228-238.
7. S. Ross and J. P. Olivier, *On Physical Adsorption*, Interscience Publishers, 1964.
8. K. Li, J. Jiang, S. Tian, F. Yan and X. Chen, *Journal of Materials Chemistry A*, 2015, **3**, 2166-2175.
9. R. Sanz, G. Calleja, A. Arencibia and E. Sanz-Perez, *Applied Surface Science*, 2010, **256**, 5323-5328.
10. R. Sanz, G. Calleja, A. Arencibia and E. S. Sanz-Perez, *Microporous and mesoporous materials*, 2012, **158**, 309-317.
11. X. Xu, C. Song, J. M. Andresen, B. G. Miller and A. W. Scaroni, *Energy & Fuels*, 2002, **16**, 1463-1469.
12. B. Singh and V. Polshettiwar, *Journal of Materials Chemistry A*, 2016, **4**, 7005-7019.
13. A. Goepfert, S. Meth, G. S. Prakash and G. A. Olah, *Energy & Environmental Science*, 2010, **3**, 1949-1960.